Electrochemistry Communications 81 (2017) 29–33

Contents lists available at ScienceDirect

Electrochemistry Communications

journal homepage: www.elsevier.com/locate/elecom

Tailoring the morphological properties of anodized Ti_3SiC_2 for better power density of Li-ion microbatteries

Alexander T. Tesfaye[a,b], Yury Gogotsi[c], Thierry Djenizian[b,d,*]

[a] Aix-Marseille Université, CNRS, MADIREL Laboratory, UMR 7246, 13397 Marseille, France
[b] FR CNRS 3104, ALISTORE-ERI, F-80039 Amiens, France
[c] Department of Materials Science and Engineering, A. J. Drexel Nanomaterials Institute, Drexel University, Philadelphia, PA 19104, United States
[d] IMT Mines Saint-Etienne, Center of Microelectronics in Provence, Department of Flexible Electronics, F - 13541 Gardanne, France

ARTICLE INFO

Keywords:
Anodized Ti_3SiC_2
Anode
Pseudocapacitance
Bulk diffusion
Li-ion microbatteries

ABSTRACT

In this work, it is reported that the morphology of negative electrodes based on anodized Ti_3SiC_2 has a strong influence on the electrochemical performance of Li-ion microbatteries. Ti_3SiC_2 was anodized in an aqueous electrolyte containing hydrofluoric acid to form an oxide film. Two typical porous structures produced at low and high applied potentials were examined by scanning electron microscopy and characterized by X-ray diffraction, mercury intrusion porosimetry, and electrochemical techniques. The power density delivered by the nanolayered structure obtained at 10 V is almost 3 times higher than that obtained from a mesoporous material formed at 60 V. Cyclic voltammetry has been used to explain that this enhanced electrochemical property is related to the higher amount of Li^+ stored at the surface of the nanolayered structure.

1. Introduction

Li-ion batteries (LIBs) have been widely used as energy storage devices in microelectronics [1–3]. However, the demand for high energy, power capability, low-cost, and safe LIBs drives the research for new electrode and electrolyte materials [4,5]. In recent years, substantial efforts have been made toward the development of nanostructured electrode materials for LIBs because of the superior electrochemical performances [2,6–8]. Recently, we reported on the fabrication and electrochemical performance of a new nanostructured anode material for Li-ion microbatteries (μLIBs) obtained by anodization of a Ti_3SiC_2 MAX phase [9]. We reported that two typical morphologies could be obtained by varying the applied potential; at a low potential (10 V), a nanolayered structure was obtained, while at a high potential (60 V), a mesoporous structure was formed. A mix of the two morphologies was observed at 30 V. MAX phases are a large family of 70 + layered ternary metal carbides and/or nitrides with composition of $M_{n+1}AX_n$: where M is an early transition metal; A is an A-group element; X is carbon and/or nitrogen; and n can be 1, 2, or 3 [10]. The anodized Ti_3SiC_2 (henceforth referred to as A-Ti_3SiC_2) shows promising electrochemical performance [11–13]. In this work, we report that the morphology of anodized Ti_3SiC_2 has a strong influence on the electrochemical performance of LIBs. Actually, the power density delivered by the nanolayered structure is almost 3 times higher than that obtained from the mesoporous material. A detailed electrochemical study has been performed to explain that this enhanced electrochemical property is related to the higher amount of Li^+ stored at the surface of the nanolayered structure.

2. Experimental

A polished and cleaned fully dense Ti_3SiC_2 was electrochemically anodized in aqueous 1 M H_3PO_4 + 1 M NaOH electrolyte containing 0.1% vol. HF for 3 h at applied potentials of 10 V and 60 V. Anodic applied potentials leading to high electrical fields (> 10 V/μm) are required to ensure the migration of oxidized species and achieve the formation of a thick oxide layer. The anatase phase was obtained by annealing the as-formed A-Ti_3SiC_2 at 450 °C in air for 3 h.

The cyclic voltammetry (CV) and galvanostatic charge-discharge tests were performed using two-electrode Swagelok cells. The half-cells were assembled by using the as-formed A-Ti_3SiC_2 film grown on the conducting Ti_3SiC_2 support as the working electrode, and Li foil as a reference electrode. A Whatman glass microfiber paper soaked in 1 M $LiPF_6$ in EC:DEC electrolyte was used as a separator. The galvanostatic charge-discharge tests were performed at 200 μA cm^{-2} in the potential window of 1–3 V vs. Li/Li^+. The CV experiments were carried out at various scan rates (0.05–1.3 mV s^{-1}) in the potential window of 1–3 V vs. Li/Li^+.

* Corresponding author at: Ecole Nationale Supérieure des Mines de Saint-Etienne, Flexible Electronics Department, CMP, 13 541 Gardanne, France.
E-mail addresses: yg36@drexel.edu (Y. Gogotsi), thierry.djenizian@mines-stetienne.fr (T. Djenizian).

http://dx.doi.org/10.1016/j.elecom.2017.05.010
Received 4 April 2017; Received in revised form 9 May 2017; Accepted 15 May 2017
Available online 16 May 2017

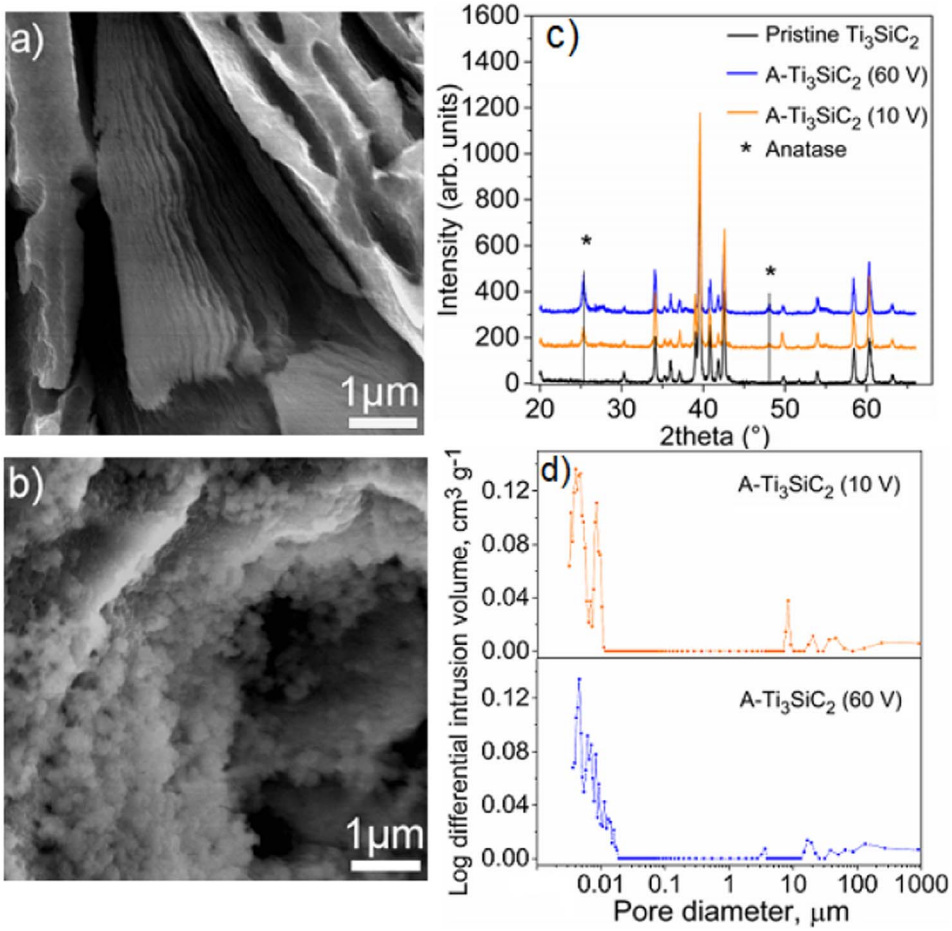

Fig. 1. SEM images of Ti_3SiC_2 anodized in 1 M H_3PO_4 + 1 M NaOH containing 0.1% vol. HF for 3 h at (a) 10 V and (b) 60 V. (c) Corresponding XRD patterns and (d) plots of the log differential intrusion volume as a function of pore diameter.

The morphology of the A-Ti_3SiC_2 was characterized by a field-emission scanning electron microscope (FE-SEM, Philips XL-30 FEG SEM). The structures were investigated by X-ray diffraction (XRD) using a Siemens D5000 diffractometer. Mercury intrusion porosimetry (MIP), Pore Master 60 QuantaChrome, was used to determine the pore size and pore fraction.

3. Results and discussion

The oxide morphology formed after the anodization of Ti_3SiC_2 is governed by the competition between electrochemical oxide formation and chemical dissolution [9]. At the low applied potential, the A-Ti_3SiC_2 – has adopted a nanolayered structure with a thickness of 3 μm (Fig. 1a), while a porous morphology with a thickness of 21 μm is obtained at the high potential (Fig. 1b). It can be noticed that as Ti is a valve metal, the thickness of the oxide layer increases with the applied potential. Similar anodization conditions were used to fabricate self-standing TiO_2 nanotubes [14].

Fig. 1c shows the XRD patterns for the pristine and anodized at 10 V and 60 V Ti_3SiC_2. The peaks at 25.19° and 48.01° correspond to the (101) and (200) reflections of anatase, respectively. The anatase phase has a structure of tetragonal with the space group of *$I4_1/amd$* and crystal size of 17 nm (JCPD file no. 21-1272). Fig. 1d shows the plots of the log differential intrusion volume as a function of pore diameter. A-Ti_3SiC_2 (60 V) has an average pore size of 5 nm with a porosity of ~20%. A-Ti_3SiC_2 (10 V) reveals 11 nm and 4 nm pores and total porosity of 35%.

In agreement with previous reports, the two CV curves (Fig. 2a and b) exhibit well-defined cathodic and anodic peaks at 1.67 and 2.17 V vs. Li/Li^+, respectively, that correspond to lithium insertion/extraction potentials in anatase. The reversible insertion/extraction of Li^+ process is given by Eq. (1) [15,16].

$$TiO_2 + xLi^+ + xe^- \rightleftharpoons Li_xTiO_2 \quad (1)$$

The mole fraction of inserted lithium (x) into anatase is close to 0.5 and corresponds to a theoretical specific capacity of 168 mAh g^{-1} [15,17]. Higher current densities are obtained for A-Ti_3SiC_2 (60 V) due to the formation of a thicker porous oxide layer during the anodization of Ti_3SiC_2 at applied potential of 60 V. The total charge stored in A-Ti_3SiC_2 is strongly dependent on the scan rate. As shown in Fig. 2, increasing the scan rate results in the increase of peak current values as well as broadening and shifting of peak positions to lower and higher potentials. These electrochemical behavior results from kinetic limitations to the diffusion of Li^+ within titania and the ohmic drop effects [13,18,19].

Fig. 2c shows the first galvanostatic charge-discharge profiles. The insertion/extraction voltage plateaus are consistent with the redox peaks observed in the CVs. The first discharge capacity values are very close, i.e. 24 μAh cm^{-2} μm^{-1} and 22 μAh cm^{-2} μm^{-1} for A-Ti_3SiC_2 (10 V) and A-Ti_3SiC_2 (60 V), respectively. Fig. 2d shows the electrochemical performance of A-Ti_3SiC_2 electrodes performed at the same kinetic for 30 cycles. The capacity loss after the first cycle can be induced by the irreversible reaction of Li^+ with trace water molecules, Li^+ trapping within the structural defects of titania, and the formation of a solid electrolyte interphase (SEI). The last discharge capacity values are 29 μAh cm^{-2} μm^{-1} and 18 μAh cm^{-2} μm^{-1} for A-Ti_3SiC_2 (10 V) and A-Ti_3SiC_2 (60 V), respectively. To compare the electrochemical performance of the two samples at a current density of 200 μA cm^{-2} after 30th cycle, a Ragone plot (Fig. 3e) has been established using data given in Table 1.

Compared to the mesoporous structure, the porous nanolayered morphology delivers a higher power density that can be attributed to

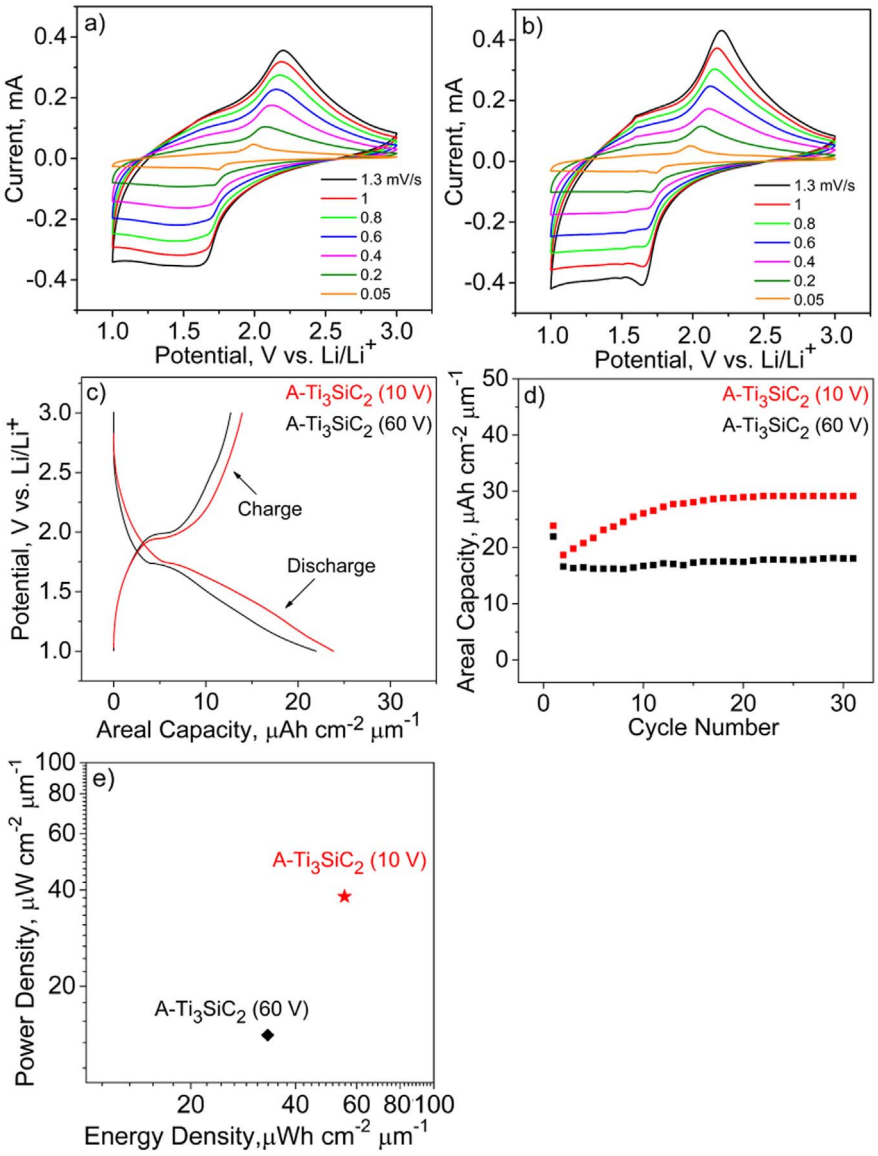

Fig. 2. (a) Cyclic voltammograms of Ti_3SiC_2 anodized at (a) 10 V and (b) 60 V recorded at various scan rates (0.05–1.3 mV s^{-1}). (c) The first galvanostatic charge-discharge profiles, (d) cycling performance and (e) Ragone plot for Ti_3SiC_2 anodized at 10 V and 60 V at a current density of 200 μA cm^{-2} after 30 cycles. All the tests were carried out in the potential window of 1–3 V vs. Li/Li^+.

the higher surface area enhancing the storage of charge through a pseudocapacitive mechanism.

CV is a powerful technique for identifying the respective contributions of the surface (pseudocapacitive effect) and the bulk (diffusion of Li^+ into the TiO_2 lattice) [19,20]. Generally, for mixed Li^+ storage processes the peak current (I*p*) is given by Eq. (2) [17,19,21].

$$Ip = C_1 v + C_2 v^{1/2} \quad (2)$$

The first term ($C_1 v$) corresponds to the pseudocapacitive current Ic, which has a linear dependence on the scan rate v; the parameter C_1 is the product of the electrode surface area A and the capacitance per electrode surface area. The second term ($C_2 v^{1/2}$) corresponds to the diffusion current I_d, which has a square root dependence on the scan rate; the parameter C_2 is given by the product of 0.4958 $nFAc(D\alpha nF/RT)^{1/2}$; where n is the number of electrons, F is the Faraday constant, c is the concentration of Li^+, D is the diffusion coefficient of Li^+, α is the transfer coefficient, R is the ideal gas constant, and T is the temperature [22]. Thus, the relative contribution of pseudocapacitive and bulk diffusion currents to the total storage current can be established by determining C_1 and C_2 at a specific scan rate.

Fig. 3a shows the peak discharge current as a function of scan rate for A-Ti_3SiC_2 (10 V). The best fit of the experimental data to an apparent power law ($Ip = a * v^b$) gives a dependence of $Ip \alpha v^{0.845}$. There are two well-defined conditions: $b = 0.5$ and $b = 1$ corresponding to pure pseudocapacitive current (dashed black line) and pure diffusion current (dashed red line), respectively. An exponent value b equal to 0.845 is attributed to the contribution of both storage mechanisms. The best fit of the experimental data to Eq. (2) is represented by the red solid line giving the values for $C_1 = 0.159 \pm 0.03$ and $C_2 = 0.00356 \pm 0.00127$. Fig. 3b shows the calculated values of Ic and I_d as a function of scan rate for A-Ti_3SiC_2 (10 V).

At low scan rates (< 0.4 mV s^{-1}), bulk diffusion of Li^+ into anatase is the predominant storage mechanism, e.g. the ratio I_d: Ic is 3:1 at 0.05 mV s^{-1}. However, the contribution of the pseudocapacitive current increases with increasing scan rate suggesting that storage of charges occurs predominately at the surface for faster kinetics. This might be the result of the extended layered morphology of A-Ti_3SiC_2 (10 V) as the contribution of pseudocapacitive storage increases with the surface area. The difference in charge storage mechanisms becomes more prominent at higher scan rates because of the fast charge/discharge processes induced by capacitive reactions, e.g. the I_d: Ic ratio is 1:1.6 at 1.3 mV s^{-1}.

Fig. 3c shows the peak discharge current as a function of scan rate for A-Ti_3SiC_2 (60 V). The best fit of the experimental data to an apparent power law gives the dependence of the peak current to the scan rate $Ip \alpha v^{0.6}$. The exponential value of 0.6 shows intercalation of Li^+

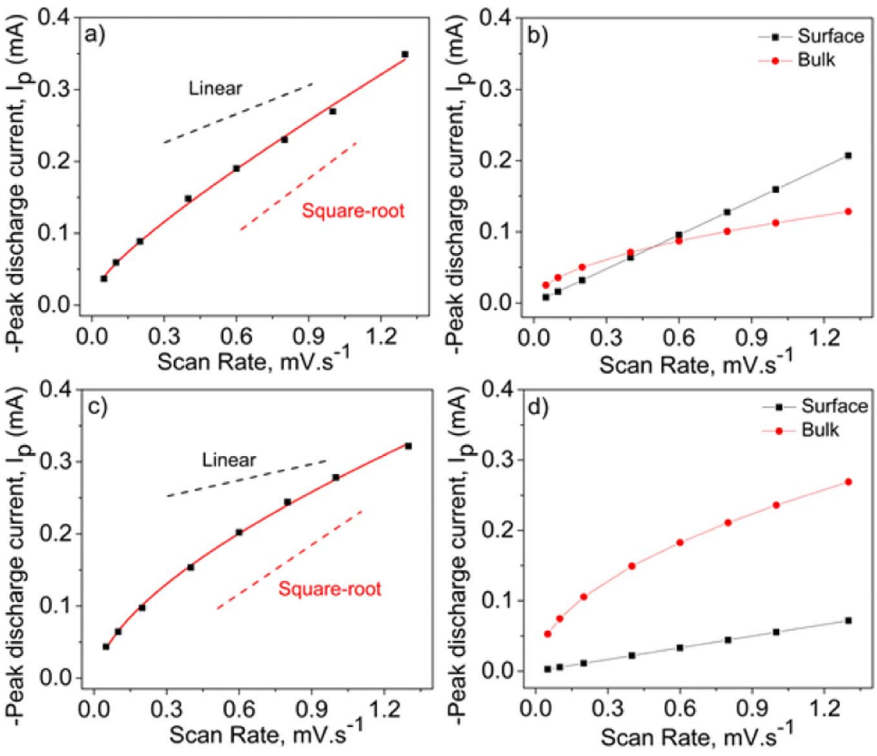

Fig. 3. (a) Peak discharge current vs. scan rate: (■) experimental data and (—) fitting for (a) A-Ti_3SiC_2 (10 V) and (c) A-Ti_3SiC_2 (60 V). Calculated surface pseudocapacitive and bulk diffusion discharge currents for (b) A-Ti_3SiC_2 (10 V) and (d) A-Ti_3SiC_2 (60 V).

Table 1
Data to establish the Ragone plot.

	A-Ti_3SiC_2 (10 V)	A-Ti_3SiC_2 (60 V)
30th discharge capacity (μAh cm^{-2} $μm^{-1}$)	29	18
Operating voltage (V)	1.9	1.84
Discharge time (h)	1.45	2.36
Energy density = discharge capacity ∗ operating voltage (μWh cm^{-2} $μm^{-1}$)	55	33
Power density = energy density/discharge time / (μW cm^{-2} $μm^{-1}$)	38	14

into the titania lattice is the dominant storage mechanism. The best fit of the data to Eq. (2) yields $C_1 = 0.0552 \pm 0.017$ and $C_2 = 0.0107 \pm 0.0007$. Fig. 3d shows that for A-Ti_3SiC_2 (60 V) bulk diffusion is the principal storage mechanism for all scan rates. The reasons for the enhanced power density can be explained by these results confirming that the layered structure formed at 10 V is able to store more charge at the surface than the mesoporous morphology obtained at 60 V.

4. Conclusion

The electrochemical performance of anodized Ti_3SiC_2 has been studied. Compared to the mesoporous morphology obtained at 60 V, the power density delivered by the layered structure formed at 10 V is almost tripled. This effect can be explained by a higher porosity of the nanolayered structure promoting the charge storage at the surface. According to CV experiments, the contribution of pseudocapacitive storage increases with scan rate and become the dominant mechanism at faster kinetics for nanolayered structure whereas for mesoporous morphology, bulk diffusion is the principal storage mechanism for the entire scan rates.

Acknowledgements

This work is financially supported by ALISTORE-ERI. T.D. and Y.G. acknowledge Master for Energy Storage and Conversion (MESC) Erasmus Mundus Program for financial support. Ti_3SiC_2 for this study was kindly provided by Prof. M.W. Barsoum, Drexel University.

References

[1] M. Armand, J.M. Tarascon, Building better batteries, Nature 451 (2008) 652–657.
[2] A.S. Arico, P. Bruce, B. Scrosati, J.M. Tarascon, W. van Schalkwijk, Nanostructured materials for advanced energy conversion and storage devices, Nat. Mater. 4 (2005) 366–377.
[3] B.L. Ellis, P. Knauth, T. Djenizian, Three-dimensional self-supported metal oxides for advanced energy storage, Adv. Mater. 26 (2014) 3368–3397.
[4] P. Poizot, S. Laruelle, S. Grugeon, L. Dupont, J.M. Tarascon, Searching for new anode materials for the Li-ion technology: time to deviate from the usual path, J. Power Sources 97–98 (2001) 235–239.
[5] H. Wu, G. Chan, J.W. Choi, I. Ryu, Y. Yao, M.T. McDowell, S.W. Lee, A. Jackson, Y. Yang, L. Hu, Y. Cui, Stable cycling of double-walled silicon nanotube battery anodes through solid-electrolyte interphase control, Nat. Nano. 7 (2012) 310–315.
[6] A.T. Tesfaye, R. Gonzalez, J.L. Coffer, T. Djenizian, Porous silicon nanotube arrays as anode material for Li-ion batteries, ACS Appl. Mater. Interfaces 7 (2015) 20495–20498.
[7] M.R. Lukatskaya, B. Dunn, Y. Gogotsi, Multidimensional materials and device architectures for future hybrid energy storage, Nat. Commun. 7 (2016) 12647.
[8] Y. Gogotsi, What nano can do for energy storage, ACS Nano 8 (2014) 5369–5371.
[9] A.T. Tesfaye, O. Mashtalir, M. Naguib, M.W. Barsoum, Y. Gogotsi, T. Djenizian, Anodized Ti_3SiC_2 as an anode material for Li-ion microbatteries, ACS Appl. Mater. Interfaces 8 (2016) 16670–16676.
[10] M.W. Barsoum, MAX Phases: Properties of Machinable Ternary Carbides and Nitrides, John Wiley & Sons, 2013.
[11] J. Xu, M.Q. Zhao, Y. Wang, W. Yao, C. Chen, B. Anasori, A. Sarycheva, C.E. Ren, T. Mathis, L. Gomes, Demonstration of Li-ion capacity of MAX phases, ACS Energy Lett. 1 (2016) 1094–1099.
[12] G.F. Ortiz, I. Hanzu, T. Djenizian, P. Lavela, J.L. Tirado, P. Knauth, Alternative Li-ion battery electrode based on self-organized titania nanotubes, Chem. Mater. 21 (2009) 63–67.
[13] W. Wei, G. Oltean, C.W. Tai, K. Edstrom, F. Bjorefors, L. Nyholm, High energy and power density TiO_2 nanotube electrodes for 3D Li-ion microbatteries, J. Mater. Chem. A 1 (2013) 8160–8169.
[14] P. Roy, S. Berger, P. Schmuki, TiO_2 nanotubes: synthesis and applications, Angew. Chem. Int. Ed. 50 (2011) 2904–2939.
[15] L. Kavan, M. Grätzel, J. Rathouský, A. Zukalb, Nanocrystalline TiO_2 (anatase) electrodes: surface morphology, adsorption, and electrochemical properties, J. Electrochem. Soc. 143 (1996) 394–400.
[16] G. Zhang, H.B. Wu, T. Song, U. Paik, X.W.D. Lou, TiO_2 hollow spheres composed of highly crystalline nanocrystals exhibit superior lithium storage properties, Angew. Chem. Int. Ed. 53 (2014) 12590–12593.
[17] H. Lindström, S. Södergren, A. Solbrand, H. Rensmo, J. Hjelm, A. Hagfeldt, S.-

E. Lindquist, Li^+ ion insertion in TiO_2 (anatase). 2. Voltammetry on nanoporous films, J. Phys. Chem. B 101 (1997) 7717–7722.
[18] J. Ye, A.C. Baumgaertel, Y.M. Wang, J. Biener, M.M. Biener, Structural optimization of 3D porous electrodes for high-rate performance lithium ion batteries, ACS Nano 9 (2014) 2194–2202.
[19] N. Plylahan, A. Demoulin, C. Lebouin, P. Knauth, T. Djenizian, Mechanism study of Li^+ insertion into titania nanotubes, RSC Adv. 5 (2015) 28474–28477.
[20] J. Wang, J. Polleux, J. Lim, B. Dunn, Pseudocapacitive contributions to electrochemical energy storage in TiO_2 (anatase) nanoparticles, J. Phys. Chem. C 111 (2007) 14925–14931.
[21] K. Zhu, Q. Wang, J.H. Kim, A.A. Pesaran, A.J. Frank, Pseudocapacitive lithium-ion storage in oriented anatase TiO_2 nanotube arrays, J. Phys. Chem. C 116 (2012) 11895–11899.
[22] A.J. Bard, L.R. Faulkner, J. Leddy, C.G. Zoski, Electrochemical Methods: Fundamentals and Applications, Wiley, New York, 1980.